Plasma Chem Plasma Process (2006) 26:543–555
DOI 10.1007/s11090-006-9014-6

ORIGINAL ARTICLE

Experimental and Theoretical Studies on the Characteristics of Atmospheric Pressure Glow Discharge with Liquid Cathode

V. A. Titov · V. V. Rybkin · S. A. Smirnov · A. L. Kulentsan · H.-S. Choi

Received: 10 March 2005 / Accepted: 28 September 2005 /
Published online: 21 April 2006

Abstract This study investigated the characteristics of an atmospheric pressure air-glow discharge with a liquid cathode. Distilled water was utilized as the cathode. The electric field strength, gas temperature as well as the emission intensity of some $N_2(C^3\Pi_u \rightarrow B^3\Pi_g)$ and OH ($A^2\Sigma^+ \rightarrow X^2\Pi$) bands were measured at a discharge current ranging from 15 to 50 mA. Based upon the data obtained, the reduced electric field strength, E/N, and effective vibrational temperatures for $N_2(C^3\Pi_u, X^1\Sigma_g^+)$ and OH ($A^2\Sigma^+$) were examined. The electron energy distribution function (EEDF) and some electron parameters (average energy, electron density and rate coefficients) were obtained based on a numerical solution of the Boltzmann kinetic equation. The result showed that the EEDF was not in equilibrium and the effective vibrational temperatures for $N_2(C^3\Pi_u, X^1\Sigma_g^+)$ were essentially higher than the gas temperatures.

Keywords Atmospheric pressure plasma with liquid cathode · Emission spectrometry · Gas temperature · Electron characteristics

1. Introduction

A gas discharge excited between an external anode and an electrolyte surface as a cathode is well known [1, 2]. Nevertheless, there is limited experimental data on these systems. Gas phase studies were performed mainly to examine the irradiation spectrum of metal-containing compounds using optical emission spectroscopy (OES) analysis. Unlike conventional sources, it is relatively easy to transfer a solute into the gas phase using the

V. A. Titov · V. V. Rybkin · S. A. Smirnov · A. L. Kulentsan
Department of Microelectronic Devices and Materials Technology,
Ivanovo State University of Chemical Technology, F. Engels ave., 7, Ivanovo, 153000, Russia

H.-S. Choi (✉)
Department of Chemical Engineering, Chungnam National University,
220 Gung -dong, Yuseong-gu, Daejeon, 305-764, Korea
e-mail: hchoi@cnu.ac.kr

cathode-sputtering phenomenon of a liquid cathode. Many researchers reported that an excitation source like this allowed the analysis of many elements [3–6]. Kanzaki et al. [7] obtained very important results in the viewpoint of both application and theory. The yield of oxidative products generated was more than 7 times higher than those expected from Faraday's law. This makes this system quite attractive because it induces a different type of oxidative process in the liquid phase including the heterogeneous phase. For example, surface modification of polymeric materials in the liquid phase is also possible. However, this type of application has not been fully investigated.

It is well known that the primary process of gas activation is electron impact. Therefore, in order to analyze and interpret the process regularity, it is necessary to know the electron gas parameters including the electron energy distribution function (EEDF). Reliable experimental methods for obtaining EEDF under high-pressure plasma conditions have not been fully developed. For example, any procedures for handling the probe current-voltage characteristics as well as microwave data require *a priori* information about the EEDF form and the charged particle movement [8]. In particular, some studies [9–12] that investigated the characteristics of an air atmospheric pressure discharge with two non-metallic electrodes assumed that the EEDF was close to a Maxwellian distribution. According to their results, the electron "temperature" was Te $\approx$ 3500–4000 K. This value was obtained based on the assumption that the electron "temperature" needs to be similar to the "temperature" at the excited level of N_2 molecules. They [9, 12] estimated the electron density to be $\sim 10^{12}\,\mathrm{cm}^{-3}$ at a discharge current of 60 mA by analyzing the probe characteristics and microwave measurement results. Under the same conditions, the rotational and vibrational temperatures, which were obtained from the irradiation intensity distributions of the molecular bands in the second positive system of the N_2 molecules ($C^3\Pi_u \rightarrow B^3\Pi_g$ transition), were 2100 ± 200 K and 4200 ± 200 K, respectively.

The main aim of this study was to obtain information on the EEDF form and electron characteristics from the numerical solutions of the Boltzmann equation. In order to obtain solutions, it is necessary to know some related plasma parameters such as the mole fraction of the main gas-phase components, the total particle density, N, and electric field strength, E (more precisely, the reduced electric field strength, E/N). These parameters were obtained experimentally.

2. Experimental

2.1. Experimental set-up

Figure 1 shows a schematic diagram of the experimental set-up. The discharge cell was exposed to ambient air and there was no gas control. A DC power supply with a 30 kΩ ballast resistor was used to excite the discharge under one atmospheric pressure (AP). A high voltage (up to 4 kV) was applied between the aqueous cathode and copper anode, which was placed at the position 1–5 mm above the liquid surface. The liquid was connected to the negative pole of the power supply with a copper electrode. The distance between the anode and the liquid surface was adjustable. The discharge current was varied from 15 to 50 mA. Distilled water was used as the cathode. The emission spectra were recorded within the wavelength range of 200–850 nm using a compact multi-purpose spectrometer (grating of 600 line/mm) (Taganrog Optical Equipment Co., Russia) equipped with a FEU-106 photomultiplier tube (PMT) (Moscow Electron Lamp Co., Russia). The signals detected by the PMT were converted into voltage signals with an analog current amplifier (U5-11, Krasnodar Company of Measuring Equipment, Russia), and then recorded with an X–Y recorder (N306, Krasnodar Company of

Fig. 1 Experimental set-up

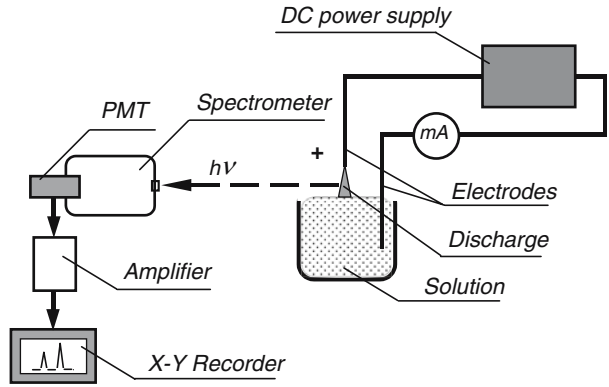

Measuring Equipment, Russia). The distance from the discharge to the spectrometer entrance slit was 55 mm. The spectral sensitivity of the optical system was measured by substituting plasma zone irradiation for the emission of a wolfram luminous element (tungsten filament band) in a SI-8-200U calibrated lamp (Moscow Electron Lamp Co., Russia) with a known luminance. The sensitivity threshold was $\sim 10^{11}$ quantum emitted in 1 cm^3 of plasma per second at $\lambda = 380$ nm.

2.2. Determination of gas temperature and $C^3\Pi_u$ (N_2), $A^2\Sigma$ (OH) "vibrational" temperatures

The rotational temperature was obtained by modelling the distribution of the emission intensity for the non-resolved rotational structure of the $N_2(C^3\Pi_u \rightarrow B^3\Pi_g, 0\text{–}2)$ band. According to the reference [13], the band structure was expressed as a superposition of the rotational line intensities of R_1, R_2, R_3, P_1, P_2, P_3, Q_2 and Q_3 branches, which overlapped due to the action of the spectrometer transfer function. It is believed that the distribution of molecules at the rotational levels is a Boltzmann distribution with the appropriate rotational temperature. The intensity factors and molecular constants were taken from the references [14–16]. The spectrometer transfer function was obtained from profile measurements of single Ne-line using a Ne-low pressure lamp as a source.

The relative band profile was calculated using temperature as a parameter. This profile was normalized to the peak intensity of the band, and was fitted using the least square method. The fitting accuracy of temperature obtained using this method was approximately ± 50 K. These errors were less than the reproducibility errors. The reproducibility errors were calculated based on five or more measurements using a confidence limit of 0.9.

Estimations revealed that under operating conditions, the rotational degrees of freedom need to be in equilibrium with the translational ones i.e. the rotational temperature and gas temperature needs to be the same.

The intensities, $I_{V',V''}$, of the $0 \rightarrow 3, 1 \rightarrow 4, 2 \rightarrow 5, 3 \rightarrow 6, 4 \rightarrow 7$ bands for the $C^3\Pi_u \rightarrow B^3\Pi_g$ transitions were obtained by integrating the appropriate band profile. The data obtained from the equation, $N_{V'} = N_{V'=0} \exp(-\Delta E_{V'}/kT_V)$, was plotted using the coordinates of $Ln[(A_{0,1}/A_{V',V''})(I_{V',V''}/I_{0,1})] = f(\Delta E_{V'})$, where $A_{V',V''}$ is the radiation probability of the appropriate transition, and $\Delta E_{V'}$ is the vibration energy for the $C^3\Pi_u$ (V') state counted off from the $V' = 0$ level. After fitting the data using the least square method, vibrational temperature, T_V, was determined from the slope of the fitting curve.

The molecular constants at the $C^3\Pi_u$ (V') state were taken from the reference [15], and the $A_{V',V''}$ values were obtained from reference [17]. The intensities of the $A^2\Sigma \rightarrow X^2\Pi(1 \rightarrow 0)$, $(0 \rightarrow 0)$ and $(2 \rightarrow 1)$ OH bands were obtained using the same method.

2.3. Measurement of electric field strength

The discharge voltage was measured between the anode and negative electrode as a function of the distance between the anode and liquid surface. The voltage drop on the water layer was measured in advance. This value was then subtracted from the voltage measured. In any case, this voltage was negligible compared with the voltage drop at the discharge zone. The voltage-distance dependence was extrapolated to a zero distance in order to obtain the cathode drop value and electric field strength (E) in the plasma column.

2.4. Calculation of electron characteristics and vibrational temperature for $N_2(X^1\Sigma_g^+)$ ground state

As reported by Gordiets et al. [18], it was assumed that the population of the different $C^3\Pi_u$ vibrational states was accomplished by electron impact from the vibrational levels of the $X^1\Sigma_g^+$ ground states. However, unlike Gordiets et al. [18], it was also assumed that the main destruction process of the $C^3\Pi_u$ vibrational states was not radiation decay but quenching via collisions with the plasma forming gas molecules. Indeed, the radiation probabilities for the different $C^3\Pi_u$ states were $\sim 2\times10^7\ s^{-1}$[17], whereas the quenching rate constants by O_2, H_2O and N_2 molecules were $\sim 10^{-10}\ cm^3/s$ [19]. The quenching frequency was estimated to be $\sim 4\times10^8\ s^{-1}$ at a particle density of $4\times10^{18}\ cm^{-3}$. Applying the above assumptions, the following five equations can be written because only five transitions were observed from the $C^3\Pi_u$ ($V' = 0 - 4$) in the irradiation spectra

$$N_e \cdot N'_{V'=0} \cdot \sum_{V'} [K_{V',0} \exp(-\Delta E_{V'}/kT_{V'})] = Z_Q^{V''} \cdot N''_{V''=0} \cdot \exp(-\Delta E_{V''=0}/kT_{V''}) \quad (1)$$

$$\bullet \quad (2)$$

$$\bullet \quad (3)$$

$$\bullet \quad (4)$$

$$N_e \cdot N'_{V'=0} \cdot \sum_{V'} [K_{V',4} \exp(-\Delta E_{V'}/kT_{V'})] = Z_Q^{V''} \cdot N''_{V''=0} \cdot \exp(-\Delta E_{V''=4}/kT_{V''}), \quad (5)$$

where summation needs to include all the vibrational levels of the $X^1\Sigma_g^+$ state; $N'_{V'=0}$, $N''_{V''=0}$ are $X^1\Sigma_g^+$ and $C^3\Pi_u$, which are the concentrations at the zero vibrational level, respectively; $K_{V',V''}$ is rate constant for excitation of the $C^3\Pi_u$ V'' level from the $X^1\Sigma_g^+$ V' level as a result of electron impact; $\Delta E_{V'}$, $\Delta E_{V''}$ are the vibrational energies for the $X^1\Sigma_g^+$ and $C^3\Pi_u$ states counted off from the zero level, respectively; $T_{V'}$, $T_{V''}$ are "vibrational" temperatures for the $X^1\Sigma_g^+$ and $C^3\Pi_u$ states, respectively; N_e is the electron density and $Z_Q^{V''}$ is the quenching frequency.

The rate constants were calculated from the following equation:

$$K_{V',V''} = \sqrt{\frac{2e}{m_e}} \int_{\varepsilon(V',V'')}^{\infty} f(\varepsilon) \cdot \sigma_{V',V''}(\varepsilon) \cdot \varepsilon \cdot d\varepsilon, \quad (6)$$

where e, m_e are the electron charge and mass, respectively; $f(\varepsilon)$ is the EEDF; $\sigma_{V',V''}$ is the process cross-section and $\varepsilon(V', V'')$ is the threshold energy, ε is the electron energy. The

EEDF was calculated from the numerical solution of the Boltzmann equation (see below). The cross-sections were obtained using the approach described elsewhere [20]. As a result of analyzing the different data, it was shown that the cross-sections for the $C^3\Pi_u\,(V')$ excitation from $X^1\Sigma_g^+(V'')$ could be written as follows:

$$\sigma_{V',V''}(\varepsilon/\varepsilon(V',V'')) = |M_e|^2 \cdot q(V',V'') \cdot F(\varepsilon/\varepsilon(V',V'')),$$

where $|M_e|^2 = 38 \times 10^{-18}\,\mathrm{cm}^2$ is the square of the matrix element for the electronic transition and $q(V',V'')$ is the Frank–Condon factor of the $V' - V''$ transition; $F(\varepsilon/\varepsilon(V',V''))$ is the universal function of the ratio of the electron energy to the threshold energy.

Suppose that $Z_Q^{V''}$ values are the same, the system of equations can be solved for $T_{V'}$ by minimizing the sum of the square of the difference in the left and right sides of (1)–(5). The use of less than ten vibrational levels for the $X^1\Sigma_g^+$ state was quite sufficient for obtaining a solution.

The EEDF was obtained from the solution of the homogeneous Boltzmann equation using a two-term expansion in spherical harmonics. The collision integrals concerning the charge particle formation were written in a similar manner used for usual inelastic processes. This is possible because the electron energy losses in these processes are negligible ($< 0.01\%$) compared with the losses for other inelastic processes. This means that the Boltzmann equation can be solved independently on the charge balance equations considering that E/N and N_e were used as the fixed parameters.

With these assumptions, the Boltzmann equation has the form

$$\frac{d}{d\varepsilon}\left(\beta\frac{df}{d\varepsilon}\right) = J_e + J_{ine} + J_{ee}, \tag{7}$$

where the EEDF has the following normalization:

$$\int_0^\infty f(\varepsilon)\cdot\varepsilon^{1/2}d\varepsilon = 1.$$

In Eq. (7), β is expressed in S.I. units as follows:

$$\beta = \frac{e^2}{3}\left(\frac{E}{N}\right)^2\left(\sum_i \sigma_i^m\delta_i\right)^{-1}\varepsilon,$$

where σ_i^m is the momentum transfer cross-section for electron collisions with heavy particles i and δ_i is the mole fraction of this type of particle.

J_e is expressed in S.I. units as follows:

$$J_e = -\frac{d}{d\varepsilon}\left(kT_g\gamma\frac{df}{d\varepsilon} + \gamma\cdot f\right),$$

where T_g is the gas temperature and

$$\gamma = 2m_e\left(\sum_i \frac{\sigma_i^m\delta_i}{M_i}\right)\cdot\varepsilon^2 + 6\varepsilon\sum_i (hcB_i)\sigma_i^r\delta_i,$$

where M_i, B_i, σ_i^r are the mass, rotational constant (cm^{-1}) and rotational cross-section for heavy particle i, respectively.

The inelastic collision integral can be written as:

$$J_{ine} = \sum_j \sum_i \delta_i \left[\varepsilon \sigma_j^i(\varepsilon) f(\varepsilon) - (\varepsilon + \varepsilon_{ji}) \sigma_j^i(\varepsilon + \varepsilon_{ji}) f(\varepsilon + \varepsilon_{ji}) \right] + \sum_l \sum_m \delta_m \left[\varepsilon \sigma_l^m(\varepsilon) f(\varepsilon) - (\varepsilon - \varepsilon_{lm}) \sigma_l^m(\varepsilon - \varepsilon_{lm}) f(\varepsilon - \varepsilon_{lm}) \right],$$

where σ_j^i is the cross-section for an inelastic collision of type j electrons with a particle of type i and σ_l^m is the cross-section for the superelastic collision of a type l electron with an excited particle of a type m and ε_{ji} and ε_{lm} are the corresponding threshold energies. The superelastic cross-sections were calculated using the appropriate first order cross-sections according to the detailed balance principle.

The electron–electron collision integral has the following form:

$$J_{ee} = -\frac{1}{8\pi} \left(\frac{e^2}{\varepsilon_0} \right)^2 \delta_e Ln(\lambda) \times \frac{d}{d\varepsilon} \left[f(\varepsilon) \int_0^\varepsilon \varepsilon^{1/2} f(\varepsilon) d\varepsilon + \frac{2}{3} \frac{df}{d\varepsilon} \left(\int_0^\varepsilon \varepsilon^{3/2} f(\varepsilon) d\varepsilon + \varepsilon^{3/2} \int_\varepsilon^\infty f(\varepsilon) d\varepsilon \right) \right],$$

where $\varepsilon_0 = 8.854 \times 10^{-12}\,\mathrm{F{\cdot}m^{-1}}$, which is the electric field constant, and δ_e is the electron mole fraction. $Ln(\lambda)$ is the Coulomb logarithm that is expressed as follows:

$$Ln(\lambda) = Ln \frac{12\pi (\varepsilon_0)^{3/2} \varepsilon_a^{3/2}}{N_e^{1/2}\, e^3},$$

where ε_a is the average energy of the electrons and N_e is the electron density.

The electron density was calculated from the equation for plasma conductivity as follows:

$$j = e\, N_e\, V_D,$$

where $j = \frac{i}{\pi R^2}$ is the current density, i is the discharge current, R is the plasma column radius, $V_D = -\frac{1}{3} \left(\frac{2e}{m_e} \right)^{1/2} \left(\frac{E}{N} \right) \times \int_0^\infty \frac{\varepsilon}{\sum_i \sigma_i^m \delta_i} \frac{df}{d\varepsilon} d\varepsilon$ is the electron drift velocity.

The radius of the plasma column was obtained by measuring the radius of the glowing column using a digital camera. The square of the column radius increased in direct proportional to the increase in the discharge current but the current density increased more rapidly than the discharge current (from ~3.3 A/cm^2 at 15 mA up to ~4.8 A/cm^2 at 50 mA) and the input power density jE.

Since the solution of the Boltzmann equation depends on the electron density (through the e–e collisions) and on the $X^1\Sigma_g^+$ vibration level population (via the superelastic collisions), an iterative procedure was used for calculation. The electron densities and the effective vibration temperature at zero iterations were both equal to zero. After solving the first step of the Boltzmann equation, the electron density was obtained from the equation for plasma conductivity, and a new value for the vibration temperature was calculated by solving Eqs. (1)–(5) up to the convergence of the numerical procedure. The mathematical details of the solution are described elsewhere [21].

It is believed that the plasma forming gas consists of N_2(78.1%), O_2(21%) and Ar(0.9%) in the case of dry air. In the case of humid air, water vapor with a content that changed during calculation was added. In this condition, the N_2:O_2:Ar ratio was the same as for dry air.

The cross-sectional areas of O_2, Ar and H_2O were taken from the literature [22-24]. The set of N_2 was obtained from reference [18].

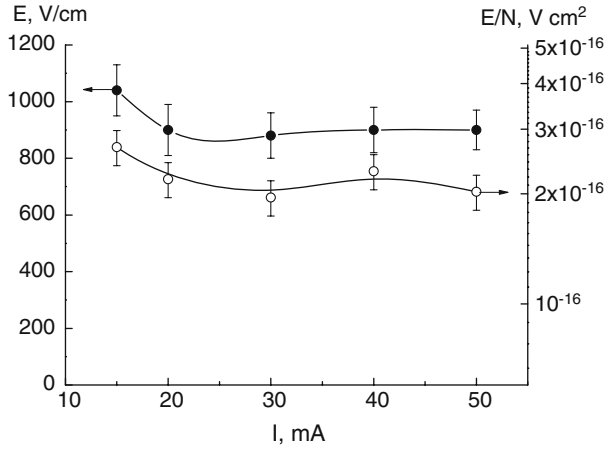

Fig. 2 Change in the electric field strength and reduced electric field strength with respect to the discharge current

3. Results and discussion

The results showed that the electric field strength was kept within a positive column under a fixed discharge current. As shown in Fig. 2, the electric field strength and the total voltage drop in the positive column were slightly decreasing functions with respect to the discharge current. Figure 2 also shows the reduced electric field strength calculated from the measured E and T values. The gas temperature obtained on the base of the rotational temperature of $N_2(C^3\Pi_u, V' = 0)$ did not depend on the discharge current (Fig. 3). The temperatures are close to those (2100 ± 200 K) reported in reference [9].

Figure 4 shows the measured intensities of the $C^3\Pi_u \rightarrow B^3\Pi_g$ bands. These intensities using the coordinates, $Ln[(A_{0,1}/A_{V',V''})(I_{V',V''}/I_{0,1})] = f(\Delta E_{V'})$, showed that the $N_2(C^3\Pi_u V')$ distribution on the vibration levels was practically Boltzmann (Fig. 5). Therefore, the use of the temperature term was correct. Figure 3 shows the $(C^3\Pi_u V')$ vibrational temperatures, which do not depend on the discharge current nor the gas temperature. The

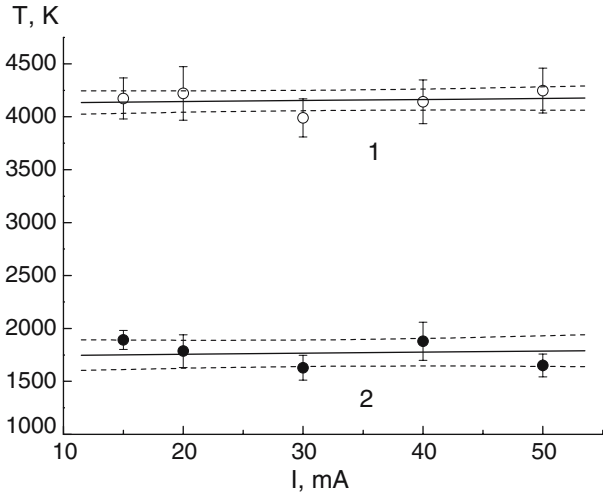

Fig. 3 Vibrational temperatures of the $N_2(C^3\Pi_u)$ state (1) and the gas temperatures (2) versus the discharge current

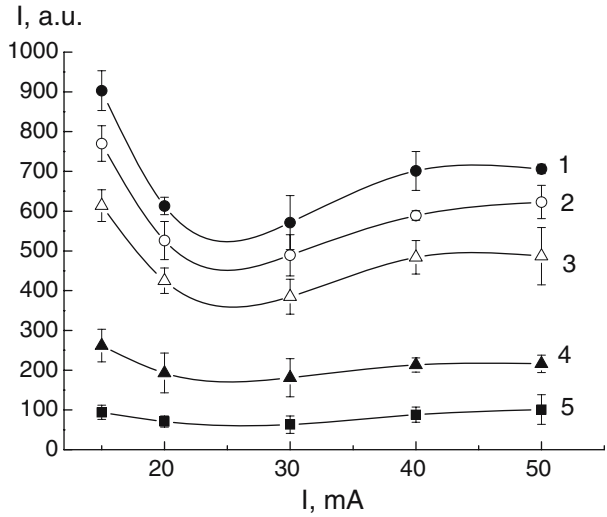

Fig. 4 The emission intensities of different bands for $C^3\Pi_u \rightarrow B^3\Pi_g$ transitions. 1, 2, 3, 4, 5 are $1 \rightarrow 4$, $0 \rightarrow 3$, $2 \rightarrow 5$, $3 \rightarrow 6$ and $4 \rightarrow 7$ transitions, respectively

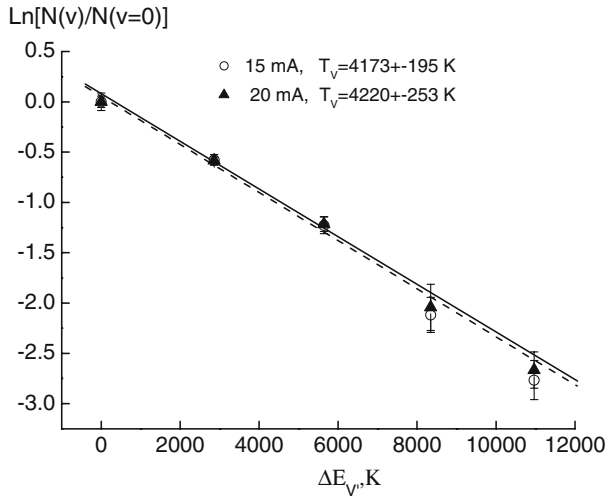

Fig. 5 Relative population of the $C^3\Pi_u$ vibrational levels versus the vibrational energy

values obtained are consistent with the data (4200 ± 200 K) reported elsewhere [9]. Similar to the ($C^3\Pi_u V'$) state, the population of $A^2\Sigma V'$ vibration levels can be characterized by the appropriate temperature. However, unlike the ($C^3\Pi_u V'$) state, this temperature shows a linear dependence on the discharge current and the changes in the gas temperature at 15 mA to ~3200 K at 50 mA (Fig. 6). In any case, this temperature is lower than for the ($C^3\Pi_u V'$) state.

The main problem with the EEDF calculation is that the molar content of water vapor is unknown. The existence of OH irradiation bands is clear evidence of water in the plasma zone. According to an indirect estimation [11], the concentration of water vapor can reach 30–40%. For this reason, two different calculations for dry air and humid air were carried out. In the latter case, the water mole fraction was set as a parameter. The effective vibration temperatures for the N_2 ground state were not affected by the presence of H_2O. The

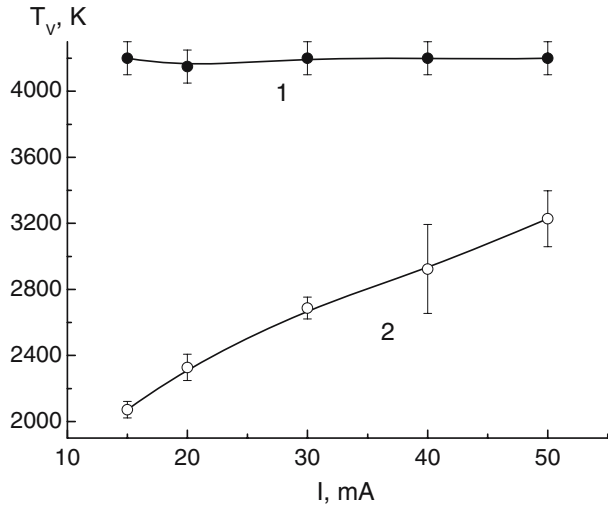

Fig. 6 Vibrational temperatures of the N_2 ground state (1) and OH ($A^2\Sigma$) vibrational temperatures (2) versus the discharge current

temperature was the same as for the ($C^3\Pi_u V'$) state and was equal to 4200±100 K (Fig. 6). Hence, the molecular distribution of the $X^1\Sigma_g^+$ lower vibrational levels is similar to that of the ($C^3\Pi_u V'$) state. If the mole fraction of H_2O is taken to be > 0.2, the average electron energy expressed in temperature units ($\varepsilon_a = \frac{3kT_e}{2}$) becomes lower than the vibration temperature. This is impossible from a theoretical point of view. For this reason, 20% is probably the upper limit of the H_2O content. However, the characteristics of the electron gas, particularly rate constants of the processes with a high threshold energy, will depend strongly on the water mole fraction. The difference between the excitation rates of the different vibrational ($C^3\Pi_u V'$) states, which were obtained from the sum of the electron impact excitation rates from ($X^1\Sigma_g^+$, V), is one order of magnitude (Figs. 7 and 8).

Nevertheless, both curves estimate the intensity dependencies of the discharge current to be similar to those measured experimentally (Fig. 4). Hence, the assumption regarding the formation-destruction processes for the ($C^3\Pi_u V'$) state is quite realistic. The curves obtained reflect the strong dependence of the EEDF "tail" on E/N. Figures 9 and 10 shows the calculated EEDF. The EEDF is similar to Maxwellian in the region of slow electrons. The main difference is observed for fast electrons. The appearance of water vapor essentially decreases the amount of high-energy electrons. This is due to the water momentum transfer cross-section larger than the cross-sections for the other plasma components. At the same time, the rate coefficients for processes with relatively low threshold energy (vibrational level excitation) slightly depend on the EEDF form. So does the electron drift velocity. Elastic collisions and vibrational level excitation are the main processes building up the EEDF under these experimental conditions. Up to 95% of the electric field energy is consumed in the process of excitation from the molecular ground states to the vibration levels through electron impact. This value does not depend on the discharge parameters. Therefore, the V–T relaxation is the main source for gas heating, and reactions involving vibration states are important for the discharge chemistry of this type. As mentioned above, the input power density increases with increasing discharge current. The action of this factor should lead to an increase in the gas temperature. However, the temperature independence on the discharge current suggests the presence of other cooling factors that have a large effect on the increase in the discharge current. This can be the increase in heat conductivity and/or heat-transfer coefficient on the

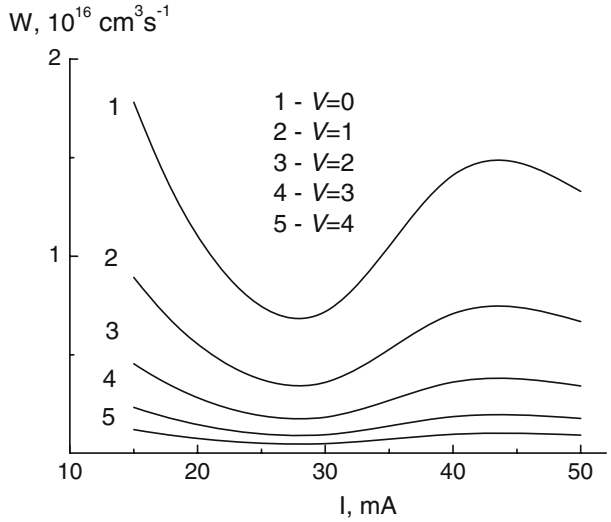

Fig. 7 The calculated excitation rates of the different $N_2(C^3\Pi_u, V)$ levels at the mole fraction of water vapor of 0.0

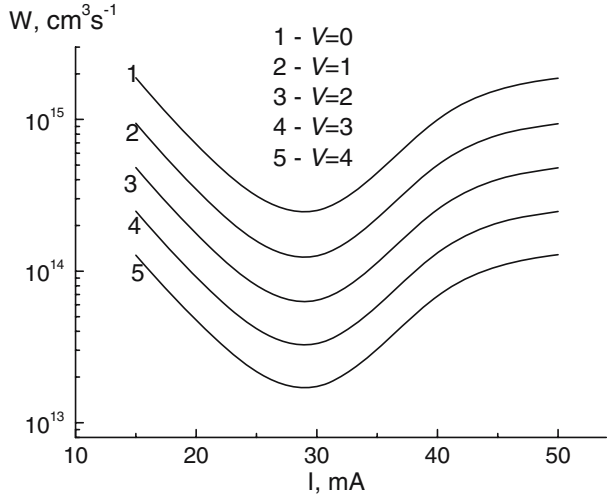

Fig. 8 The calculated excitation rates of the different $N_2(C^3\Pi_u, V)$ levels at the mole fraction of water vapor of 0.2

plasma–gas interface. The increase in water evaporation with increasing discharge current might be responsible for this effect. Nonetheless, the heat conductivity for water vapor is almost twice that for dry air [25].

For low pressure plasma in air, the $(X^1\Sigma_g^+, V)$ vibrational temperature slightly depends on the pressure at a fixed discharge current and strongly depends on the discharge current at a fixed pressure [18, 26]. This is due to an increase in the electron pumping frequency, which is faster than the V–T exchange frequency. However, in our case, the increase in the electron density (Fig. 11) with increasing discharge current from 15 mA to 30 mA does not result in an increase in the $N_2(X^1\Sigma_g^+)$ vibrational temperature. This is possible if the main reason for forming and destroying the vibrational level is electron impact. Indeed, the K_{10} rate coefficient for the N_2 V–T relaxation at 2000 K is 1.4×10^{-15} cm^3/s [27]. The V–T relaxation frequency was calculated to be 5×10^3 s^{-1} by taking the particle density to be

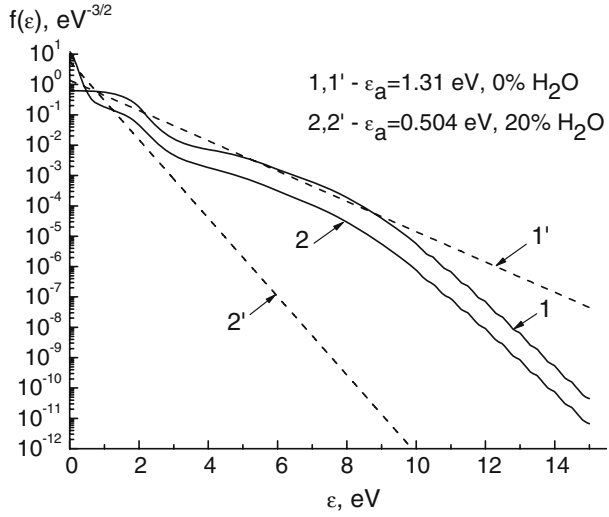

Fig. 9 Calculated EEDF (1, 2) at the15 mA discharge current. The dotted lines ($1', 2'$) are the Maxwellian EEDF with the same average energy as for the calculated EEDF

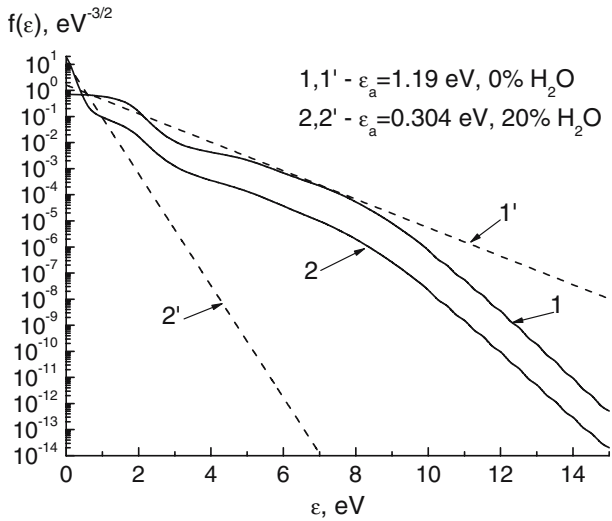

Fig. 10 Calculated EEDF (1, 2) at the 30 mA discharge current. Dotted lines ($1', 2'$) are the Maxwellian EEDF with the same average energy as for the calculated EEDF

$3.9 \times 10^{18}\,\mathrm{cm}^{-3}$. At the same time, the deactivation rate coefficient of the $V = 1$ level as a result of electron impact was $K_{10}^{e} \approx 6 \times 10^{-9}\,\mathrm{cm}^3/\mathrm{s}$. At an electron density of $6 \times 10^{12}\,\mathrm{cm}^{-3}$, the appropriate deactivation frequency is approximately $4 \times 10^4\,\mathrm{s}^{-1}$. A study [27] reported that, in the case of the Boltzmann vibrational distribution and the Maxwellian form of EEDF, the electron temperature needs to be equal to the vibrational one on account of the balance between the forward and backward processes $e + M_2(V = 1) \overset{K_{10}, K_{01}}{\longleftrightarrow} e + M_2(V = 0)$, where K_{01}, K_{10} are the rate coefficients of the electron impact excitation of the forward and backward processes, respectively. Using the rate coefficients and the relation, $N_e N(V = 1) K_{10} = N_e N(V = 0) K_{01}$, it is possible to estimate the effective temperature, T_{eff}, to be $N(V = 1)/N(V = 0) = K_{01}/K_{10} = \exp(-\Delta E_{10}/T_{\mathrm{eff}})$. $T_{\mathrm{eff}} = 5500\,K = 0.48\ eV$ was obtained using $K_{01} = 3.3 \times 10^{-9}\,\mathrm{cm}^3/\mathrm{s}$, $K_{10} = 6 \times 10^{-9}\,\mathrm{cm}^3/\mathrm{s}$ and $\Delta E_{10} = 3393\,K \approx 0.3\ eV$.

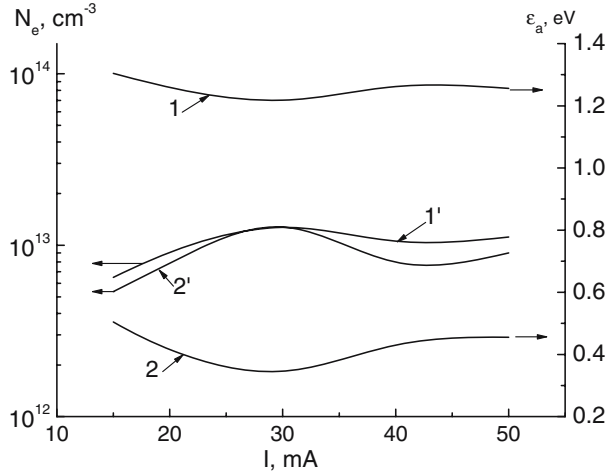

Fig. 11 Calculated parameters of electrons. 1, 2 are the average energy, $1'$, $2'$ are the electron density. 1, $1'$ — water vapor mole fraction is equal to zero. 2,$2'$ -water vapor mole fraction is equal to 0.2

At the Maxwellian form of EEDF, the T_{eff} value can be related to the average electron energy, ε_a, in the form of $T_{\text{eff}} = 2\varepsilon_a/3$. Thus, $\varepsilon_a = 0.72$ eV. Certainly, the EEDF is not Maxwellian but the vibrational level excitation processes have a low threshold energy (0.3 eV for $0 \rightarrow 1$ transition) and the low energy EEDF part is responsible for the rate coefficients. However, in this region, the EEDF is close to a Maxwell distribution. At least, the difference between the estimated T_{eff} value of 5500 K and the experimental value of 4200 K is not great. Moreover, the value, $\varepsilon_a = 0.72$ eV, can be obtained if it is assumed that the water mole fraction is $< 20\%$ (see Fig. 11).

Unfortunately, no quantitative explanations on the OH vibrational temperatures could be made due to the lack of appropriate kinetic data. It is possible that the OH radical forms as a result of H_2O dissociation via electron impact followed by excitation into the $A^2\Sigma$ state. The process of dissociative excitation by electron impact is improbable due to the high threshold energy needed, $H_2O + e \rightarrow OH(A^2\Sigma) + H(^2S) + e$, $\varepsilon_{ex} \approx 9.2$ eV. Unlike the emission of N_2, $C^3\Pi_u \rightarrow B^3\Pi_g$, the intensities of the OH ($A^2\Sigma$) bands increased with increasing discharge current in the same manner as the OH vibrational temperature shown in Fig.6. Due to the high threshold energy ($\varepsilon_{ex} \approx 4.1$ eV), the OH ($A^2\Sigma$) excitation frequency via electron impact cannot increase. Therefore, this increase is related to the increase in the water concentration. The proximity of the gas temperature and OH vibrational temperature suggests that the V–T relaxation process plays an important role. If main plasma forming gases except water vapor participate in these processes, then the increase in the OH vibrational temperature can be related to the increase in the excitation frequency for the OH vibrational levels due to the increase in the electron and water vapor concentration with increasing discharge current.

4. Conclusions

Experimental data showed that atmospheric pressure air glow discharge was a non-equilibrium system. The vibrational temperatures of some plasma components are higher than the gas temperatures. The EEDF was different from the Maxwell distribution, particularly in the region of fast electrons. However, the N_2 ground state vibrational temperature was

close to the average electron energy in appropriate units. Elastic collisions and vibrational level excitations were the main processes for building up the EEDF under these experimental conditions. The plasma properties strongly depend not only on the original plasma forming gases but also on the transfer processes from the liquid to gas phase.

Acknowledgments This work was supported by the Korean Organization of Science and Engineering Foundation Grant for Local Laboratory Project (KOSEF-2004-0150).

References

1. Davies RA, Hickling A (1952) J Chem Soc 3595
2. Hickling A, Linacre JK (1954) J Chem Soc 711
3. Brisset JL, Lelievre J, Amouroux J (1990) Rev Phys Appl 25:535
4. Cserfalvi T, Mezei P, Apai P (1993) J Phys D: Appl Phys 26:2184
5. Cserfalvi T, Mezei P, Fresenius (1996) J Anal Chem 355:813
6. Davis WC, Marcus RK (2001) J Anal At Spectrom 16:931
7. Kanzaki Y, Nishimura N, Matsumoto O (1984) J Electroanal Chem 167:297
8. Huddlestone RH, Leonard SL (1965) Plasma diagnostic techiqiues, Academic Press, New-York-London
9. Faure G, Shkol'nik SM (1998) J Phys D 31:1212
10. Andre P, Aubreton Yu. Barinov J, Elchinger MF, Fauchais P, Faure G, Kaplan V, Lefort A, Rat V, Shkol'nik S (2002) J Phys D 35:1846
11. Barinov YuA, Shkol'nik SM (2002) Technical Phys 47:313
12. Barinov YuA, Kaplan V, Rozhdestvenkii VV, Shkol'nik S Technical Phys Lett 24:929
13. Herzberg G (1950) Spectra and molecular structure: Spectra of diatomic molecules. D.Van Nostrand Co., Princeton
14. Kovacs J (1969) Rotational structure in the spectra of diatomic molecules. Academiai Kiado, Budapest
15. Huber KP, Herzberg G (1979) Molecular spectra and molecular structure: constants of diatomic molecules. Van Nostrand-Reinhold, New York
16. Laher RR, Gilmore FR (1991) J Phys Chem Ref Data 20:695
17. Nicholls RW (1964) Ann Der Geophys 20:144
18. Gordiets BF, Ferreira CM, Guerra VL, Loureiro J, Nahoroy J, Pagnon D, Touzeau M, Vialle M (1995) IEEE Trans Plasma Sci 23:750
19. Pancheshnyi SV, Starikovskaia SM, Starikovskii AYu (1998) Chem Phys Lett 294:523
20. Slovetski DI (1980) Mechanism of chemical reactions in the nonequilibrium. Nauka, Moscow
21. Diamy A-M, Legrand J-C, Rybkin VV, Smirnov SA (2005) Contr Plasma Phys 45:3
22. Kajita S, Ushiroda S, Kondo Y (1990) J Appl Phys 67:4015
23. Kieffer J (1973) Comparison of Electron Collision Cross-Section Data for Modeling Gas Discharge Lasers, Join. Instr. for Lab. Astrophys. Univ. of Colorado, Rep.13
24. Shimamura I (1989) Papers I.R.C.R. (Japan) 82:1
25. Grigoriev IS, Meilihov EZ (ed) (1991) Handbook of physical values, Atomizdat, Moscow [in Russian]
26. Smirnov SA, Rybkin VV, Kholodkov IV (2002) High Temperature 40:161
27. Capitelli M (ed) (1989) Nonequilibrium vibrational kinetiks. Springer-Verlag, Berlin Heidelberg, New-York, London, Paris, Tokyo